Ultrafast charge division imaging detector

Alan Liu and Brian Woo
Physical Electronics, Inc., 575 Chesapeake Drive, Redwood City, California 94063

Robert W. Odom[a)]
Charles Evans and Associates, 301 Chesapeake Drive, Redwood City, California 94063

(Received 14 December 1999; accepted for publication 25 July 2000)

We have developed position computing electronics having less than 60 ns dead times for resistive anode encoders, a form of charge division imaging detector. These electronics are at least a factor of 5 faster than anything available commercially and are based on using a fast, self-resetting charge integrator and subrange digital division techniques. Our primary application for this detector is secondary ion mass spectrometry (SIMS)/ions imaging and we demonstrate that SIMS imaging applications using these ultrafast electronics can readily be performed at ion intensities above 10^6 cps. This article discusses the overall electronics design and presents experimental data on dead-time measurements, detector lateral resolution, and SIMS imaging. © *2000 American Institute of Physics.* [S0034-6748(00)04610-4]

I. INTRODUCTION

Two-dimensional (2D), pulse counting detectors for imaging intensity distributions of charged particles, energetic neutrals, and photons often require high spatial resolution and fast pulse processing.[1] New developments in quantitative 2D detectors attempt to improve their operational characteristics under demanding performance requirements which include:

(i) single pulse counting,
(ii) dynamic range $\geqslant 10^7$,
(iii) submicrometer pixels sizes, and
(iv) image area $\geqslant 256\times 256$ pixels.

Over the past 15 yr, we have developed new electronic processing techniques[2] as well as innovative sensors for resistive anode encoders (RAEs), a charge-division imaging sensor.[3] These pulse counting, imaging devices are commonly used as ion image detectors in state-of-the-art secondary ion mass spectrometry (SIMS), as well as electron detectors in both photoelectron and Auger electron spectroscopies. In SIMS, RAEs image the intensity distributions of mass selected secondary ions sputtered from analytical surfaces. A RAE can resolve lateral distributions of secondary ions below 1.0 μm by coupling appropriate ion optics in the SIMS mass spectrometer to the image detector which provides both ion position and intensity.[4] Using appropriate sensitivity factors, secondary ion images can be converted into images of elemental concentration. Since SIMS erodes the analytical surface layer by layer, combining a pulse counting, position sensitive detector with imaging SIMS can achieve sensitive compositional analysis at sub-μm lateral and in-depth resolutions.

Our goal at the outset of this recent work was to develop RAE position computing electronics having particle detection rates ten times faster than those available on commercial systems. This goal translates into developing a fast imaging detector with a 35 ns dead time and 8-bit×8-bit position resolution.

Since no traditional pulse processing method could be readily extended to the desired speeds, we developed alternative, fast methods for performing the position calculation using fast pulse summation, ratioing, and digitization. In addition, buffering methods were developed to maximize output rates using conventional PC-compatible computer hardware. The new detection and signal processing electronics do not introduce significant distortion or artifacts into the RAE image. As demonstrated below, this research successfully developed RAE position computing electronics having dead times less than 35 ns for uniformly spaced test pulses and 60 ns dead times in SIMS ion imaging applications over image fields comprised of 256×256 pixels in X and Y. We refer to this new RAE position computer as the ultrafast RAE and its attributes are discussed in Sec. II.

II. EXPERIMENT

We utilized a conventional resistive anode encoder produced by Quantar, Inc. (Santa Cruz, CA) with a fast, low-resistance anode and hot, high current microchannel plates (MCPs). The ultrafast circuitry was developed with the RAE detector mounted on a 6 in. conflat flange bolted onto a vacuum test stand. During initial testing of the circuitry, image patterns were generated using both a movable electron source as well as an ultraviolet (UV) lamp illuminating a metal grid. This UV radiation produces a light pattern on the front surface of the first MCP from which photoelectrons are emitted, amplified, and imaged on the RAE sensor. Final tests were performed on a CAMECA IMS-3*f* ion microanalyzer which has been discussed in detail elsewhere.[5]

Figure 1 illustrates a schematic diagram of a typical RAE detector assembly comprised of a pair of microchannel

[a)]Author to whom correspondence should be addressed; electronic mail: Rodom@cea.com

 © 2000 American Institute of Physics

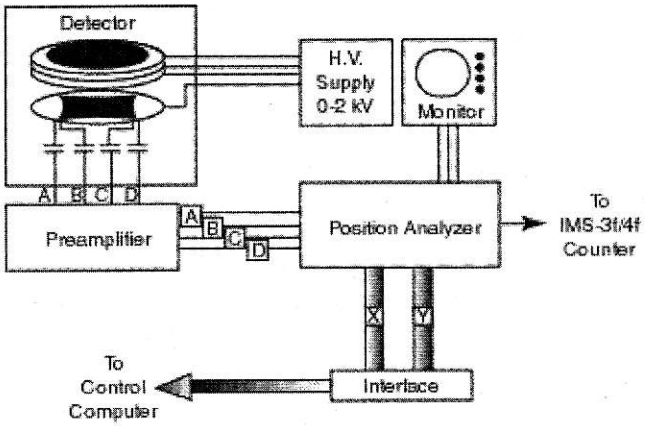

FIG. 1. Illustration of complete resistive anode encoder with microchannel plates.

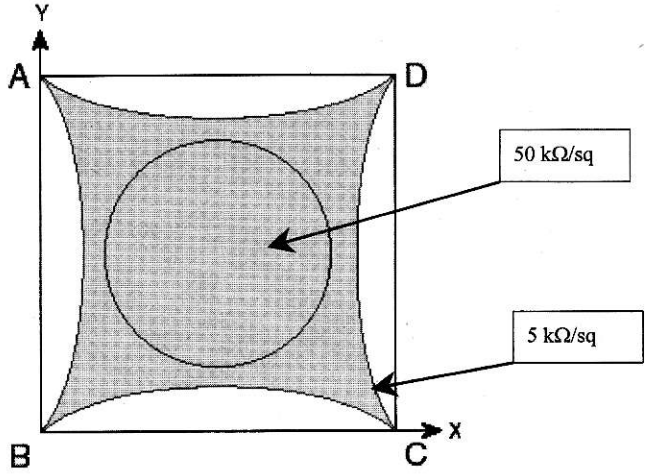

FIG. 2. Diagram of a resistive anode illustrating two different resistivity regions and the four corners where charge is collected.

plates positioned in front of the resistive anode. The collision of charged or energetic particles or the absorption of photons at the front surface of the first microchannel plate produces secondary electrons which are accelerated down the channels of the MCPs. Subsequent electron/surface collisions produce new generations of secondary electrons along the channel walls. Using typical accelerating voltages of 1kV per MCP plate, approximately 10^6 electrons are generated for each particle or photon incident on the front surface of the detector.[6] For the case of resistive anode encoders, the output electron pulse from the MCP strikes the resistive film of the anode, the corners of which are attached to four electrodes. The resistivity of the anode is shaped (Fig. 2) into a high resistance central region (50 kΩ/sq) and a lower resistance border (~5 kΩ/sq) to linearize the position response at the anode corners.[7]

The charge deposited onto the anode by a burst of electrons exiting the second MCP is collected at the four electrodes (A, B, C, D) and the total charge is the sum of the charge collected on all electrodes. The charge collected at any electrode depends on the position of the electron pulse within the 2D area of the film. X and Y positions are calculated using the following ratios:

$$\text{Total charge} = A + B + C + D, \tag{1}$$

$$X = (A + B)/(A + B + C + D), \tag{2}$$

$$Y = (B + C)/(A + B + C + D). \tag{3}$$

Two issues that complicate the position calculation are variations in charge arrival times at the four electrodes and variable pulse height distributions of the collected charges. The pulse processing electronics we developed addresses these issues by using:

(i) a self-resetting charge integrator that accommodates variable pulse arrival times at the four corners, and
(ii) a subrange digital division to accommodate the pulse height distribution with a reasonably sized circuit.

The remainder of this section describes these circuit elements as well as the details of the charge ratioing circuitry.

A. Integration and pulse shaping

The self-resetting charge integrator integrates the pulse from the output of the amplifier at each corner of the RAE and holds this charge for ~15 ns. Figure 3 illustrates the pulse characteristics of this integrator along with its circuit diagram. The integrator is reset in the following manner:

(1) Whenever a pulse is injected into the integrator (U2), the output will settle to a level corresponding to the total charge in the pulse. This level remains constant for ~15 ns.
(2) The same input pulse travels through a 20 ns delay line and is inverted by U1 before feeding into the integrator.

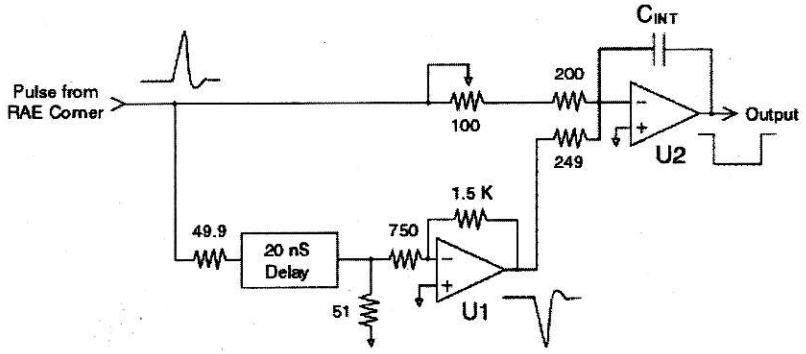

FIG. 3. Circuit diagram of the self-reset charge integrator.

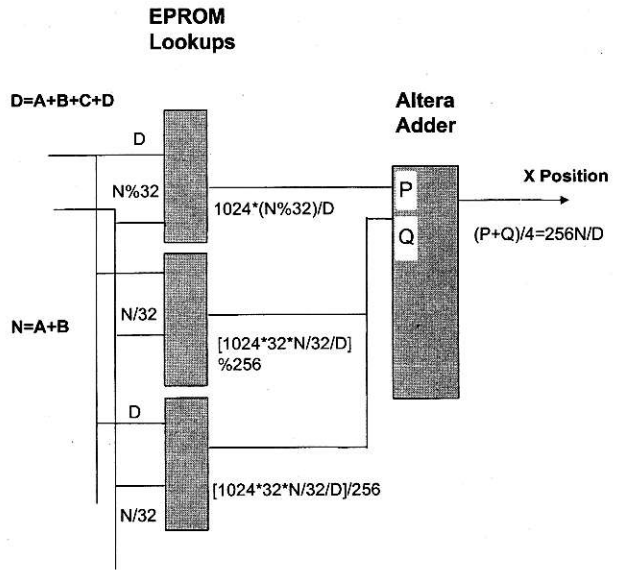

FIG. 4. Digital division circuit for ultrafast RAE.

(3) When the delayed, inverted pulse reaches the integrator, an equal and opposite signal is fed to the integrator to remove the original pulse charge, restoring the integrator to its initial level.
(4) A short plateau appears at the output of the integrator for about 15 ns which resembles the output of a sample and hold amplifier. Unlike a conventional sample and hold circuit, this integrator circuit resets itself after each pulse.
(5) The 15 ns stable output gives a 10 ns interval where all four outputs are constant for accurate summing and digitization.

The integrator is preceded by fast, low noise preamplifiers.

B. Summing, digitizing, and buffering

The integrated pulses are summed prior to digitization to form the numerator and denominator for the position calculation. Since the X position is proportional to $(A+B)/(A+B+C+D)$ and the Y position is proportional to $(B+C)/(A+B+C+D)$, only three sums are needed beyond this point.

The full sum pulse $(A+B+C+D)$ is compared against upper and lower thresholds to determine if the amplitude is acceptable for digitizing. Any pulse outside of the set range generates a signal that inhibits pulse processing. The digitization of the three sums is done by three fast, 10-bit analog to digital (A/D) converters which receive a clocking pulse from the timing circuitry to initiate the digitization.

Each A/D converter is followed by a first-in-first-out buffer having 1024 levels. Since pulses arrive randomly at the detector, we want to hold them in a buffer and subsequently process each pulse at a steady rate. The buffers are filled at the digitization rate, which is nominally the pulse arrival rate, and are emptied at 3 MHz. While a 3 MHz clock was chosen for convenience, the components can accommodate a 5 MHz clock with appropriate timing adjustments.

C. Subrange digital division

To accommodate incoming pulse height distributions, we digitize in 10 bits to give 8-bit accuracy at a pulse height distribution of 4:1. After several trials, we realized the circuit could be tremendously simplified by splitting the numerator into two parts before the digital divide, and then adding the parts together after the division. In other words, if

$$N=N_1+N_2, \tag{4}$$

then

$$\frac{N}{D}=\frac{N_1}{D}+\frac{N_2}{D}.$$

Figure 4 is a schematic of this subranging digital divide. The denominator signal is the sum of all four corner pulses, $A+B+C+D$, digitized to 10 bits. The numerator for one of the two dimensions, say X, is the sum of two corner pulses $A+B$, also digitized to 10 bits. One way to partition the calculation is to split the 10-bit numerator into the five most significant and the five least significant bits. Dividing the least significant 5 bits by the 10-bit denominator involves only 15 input bits, and the resulting output, which is 8 bits or less, can be handled by programming a standard fast erasable programmable read-only memory (EPROM) as a divider lookup table. The five most significant numerator bits along with the 10-bit denominator again comprise 15 bits, which are fed into two more EPROMS. One handles the lower 8 bits of the output, and the second handles the remaining 2 bits. At the same time, this arrangement allows the numerator to be multiplied by a factor of 4 (in the EPROM lookup table, thus the factor of $1024=4\times256$) and the final result is divided by four by simply shifting bits. This increases the precision and the calculation can be performed using only three chips.

The EPROMs were limited to 16 address bits because of the availability of suitable chips during our investigation. It

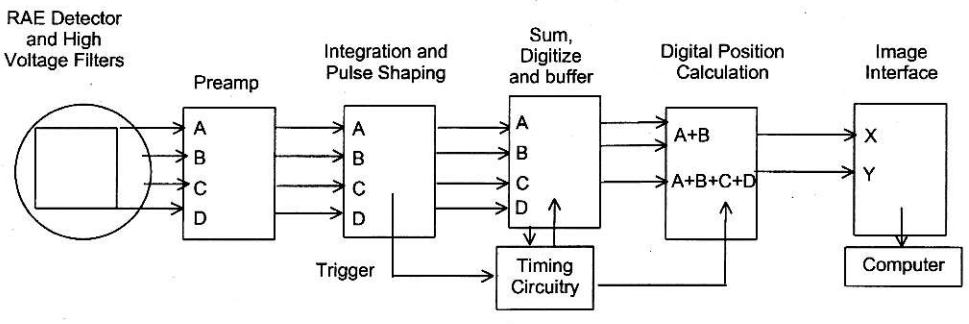

FIG. 5. Schematic of complete layout of ultrafast RAE circuit.

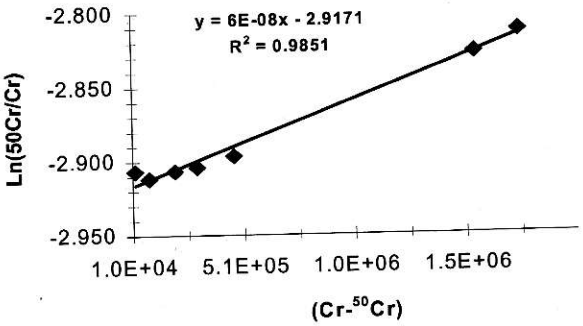

FIG. 6. Detector dead-time measurement in SIMS analysis of Cr isotope ratios illustrating 60 ns dead time.

should be possible to simply use two chips with 20-bit inputs to maintain the full precision of the division. Some improvement in precision can be gained by partitioning the numerator into 6-bit and 4-bit chunks, instead of the 5 bits and 5 bits illustrated here.

The 10 output bits of the last two EPROMS are combined, and this number is added to the 8-bit output of the first EPROM in a programmed Altera logic chip. The output is also divided by four to remove the factor previously introduced. This is done for both X and Y. The entire calculation stage requires a total of six EPROMS and one Altera chip. Figure 5 is a block diagram of the complete ultrafast RAE detector and processing electronics.

III. RESULTS AND DISCUSSION

The ultrafast RAE prototype demonstrates good image quality and resolution with minimal distortion. The electronic design delivers a pulse processing capability of 30–35 ns between pulses. The most important characteristics of this detector vis à vis existing RAE systems were evaluated on a CAMECA IMS-3f microanalyzer used for secondary ion imaging applications. Of particular interest are the following characteristics in SIMS imaging:

(i) detector dead time,
(ii) dynamic range, and
(iii) image resolution.

Detector dead time was measured by image isotope ratio analysis in which the relative intensities of images of $^{50}Cr^+$ and $^{52}Cr^+$ were determined over a 150 μm diam image field as a function of the $^{52}Cr^+$ intensity using a 12.5 keV O_2^+ primary ion beam sputtering a Cr target. The dead time is given by[2]

$$\tau \approx \ln[R_M/R_T]/(^{52}\mathrm{Cr}-^{50}\mathrm{Cr})_T, \tag{5}$$

where R_M and R_T are the measured and true $^{50}Cr/^{52}Cr$ isotope ratios, respectively, and $(^{52}Cr-^{50}Cr)_T$ is the difference in the true ion counts for the two isotopes. By keeping count rates below $\sim 3\times 10^6$ cps, the true count rate difference is approximately equal to the measured value. Figure 6 plots the logarithm of the measured $^{50}Cr/^{52}Cr$ ratios as a function of $^{52}Cr^+$ count rate using Eq. (5). Chromium isotope ratios were measured out to count rates of 1.7×10^6 cps of $^{52}Cr^+$ and the experimentally measured dead time was 60 ns. The

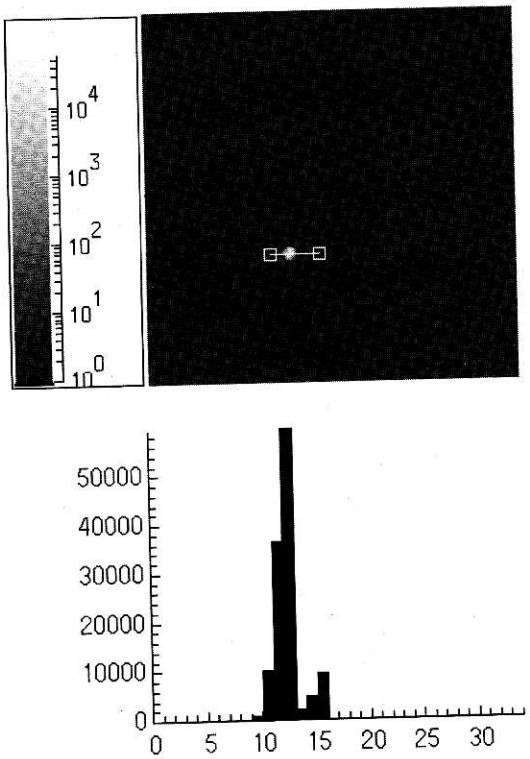

FIG. 7. Image of injected current into anode along with line scan profile of this spot.

dead time drops to ~30 ns if the $^{52}Cr^+$ count rate is kept below 10^6 cps. Thus, this new RAE circuitry has decreased the measured dead time over existing fast RAE detection electronics by factors ranging between 5 and 10 depending on the input count rate. These isotope ratio measurements also demonstrate a detector dynamic range greater than 10^6.

The discrepancy between the measured 60 ns dead time at count rates greater than 10^6 and the design dead time of 35 ns is due, most likely, to a dc base line shift of the $(A+B+C+D)$ output. At high count rates, the duty cycle at the output increases and the average dc level shifts downward so that the overall pulse amplitude appears lower when driving the upper and the lower threshold comparators. The fact that the pulses have a height distribution will cause rejection of some lower amplitude pulses under high count conditions.

To test this hypothesis, a control experiment was performed using the RAE setup on the CAMECA 3f with an electronic pulse train to simulate ions arriving at the detector. Bursts of pulses were produced using two signal generators in which one gated the other. Each pulse burst contained ~20 pulses, 4 ns wide and separated by 35 ns which were fed into a programmable divide by 1 or divide by 16 circuit. These pulses served as inputs to the four corners of the ultrafast RAE electronics. This setup simulates an isotope ratio of 1:16 and we acquired ratio data on the CAMECA software with these simulated ion counts. We also verified that the count rate detected by the RAE electronics was equal to the count rate measured on a frequency counter. We changed the input count rate by changing the burst rate and verified that the measured ratio was constant from 1000 to $>3\times 10^6$ pulses/s. This simulated ion arrival differs from an actual SIMS measurement in that the simulated pulses had

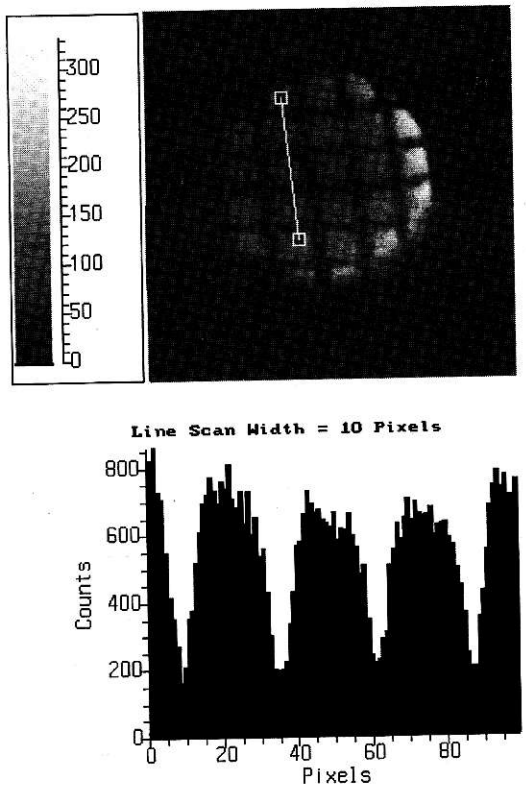

FIG. 8. SIMS secondary ion image of Al^+ acquired with ultrafast RAE electronics. Image is 150 μm in diameter and image resolution is less than 1 μm.

no height distribution (all pulses are the same height) and the 4 ns pulse widths were constant. We also adjusted the amplitude of the simulated pulses so that all the pulses were accepted by the threshold comparators even when the rate was high enough to shift the dc level of the $(A+B+C+D)$ output. These experiments demonstrate that the intrinsic dead time of the detection electronics is $\approx$35 ns.

The image resolution of the detector were evaluated offline and on a CAMECA SIMS instrument. The offline measurements consisted of pulsing currents into a resistive anode with a rigidly mounted, 20 μm diam Ta wire pressed onto the anode and measuring the size of the "image" as a function of the injection voltage (charge). Since the nominal pixel size for the RAE is $\sim$100 μm (256 pixels in a 25 mm diam sensor), the 20 μm probe is significantly smaller than the optimal resolution. Current was injected into the surface of the RAE using a fast pulse generator and 7 ns pulse widths. Figure 7 illustrates an image produced from a sum$(A+B+C+D)$ voltage of 2.78 V corresponding to the

TABLE I. Variation of detected spot size as a function of sum voltages and estimated injected charge.

Sum voltage	Injected charge (10^6 electrons)	Spot size, FWHM (pixels)
2.18	2.9	4.2
2.78	3.7	3.0
4.1	5.4	2.0

injection of $\sim 3.7\times 10^6$ electrons. The injected charge was calculated from the sum voltage using the total voltage gain in the circuit (700), its output impedance (50 Ω), and the injection pulse width. The image is displayed on a logarithmic scale and is a well-defined spot with no streaking or noise outside the central region. The lower image in Fig. 7 is a line scan through this spot illustrating that it is 3 pixels wide [full width at half maximum (FWHM)]. Varying the injection voltage effectively varies the S/N of the charge sensing circuitry of the RAE and Table I lists the results obtained for three distinct voltages. As expected, lower S/N translates into lower resolution with the best resolution corresponding to approximately 2 pixels. With regard to image resolution with the ultrafast RAE electronics, Fig. 8 illustrates a SIMS ion image of Al^+ ions generated by O_2^+ primary ion beam bombardment of a Cu grid on an aluminum substrate. The Cu wires in this grid are 5 μm in diameter and the open areas between grid wires are 25 μm$\times$25 μm. The image field is 150 μm in diameter magnified 100$\times$ in the figure and the Al^+ intensity is approximately 4×10^5 cps integrated for 10 s. The line scan plot below the ion image illustrates that the 5 μm wide Cu wires span approximately 10 pixels and thus the image resolution is on the order of 1 μm, which correlates well with the probe measurements discussed above.

ACKNOWLEDGMENT

Partial support for this research was provided by AFTAC Contract No. F09603-93-C-0033.

[1] R. W. Odom, Appl. Spectrosc. Rev. **29**, 67 (1994).
[2] R. H. Brigham, R. J. Bleiler, P. J. McNitt, D. A. Reed, and R. H. Fleming, Rev. Sci. Instrum. **64**, 420 (1993).
[3] M. Lampton and C. W. Carlson, Rev. Sci. Instrum. **50**, 1093 (1979).
[4] R. W. Odom, B. K. Furman, C. A. Evans, Jr., C. E. Bryson, W. A. Peterson, M. A. Kelley, and D. H. Wayne, Anal. Chem. **55**, 574 (1983).
[5] M. Schumacher, H. N. Migeon, and B. Rasser, in *Secondary Ion Mass Spectroscopy (SIMS-VII)*, edited by A. Benninghoven, C. A. Evans, Jr., K. D. McKeegan, H. A. Storms, and H. W. Werner (Wiley, New York, 1990).
[6] J. L. Wiza, Nucl. Instrum. Methods **162**, 587 (1979).
[7] M. Lampton and C. W. Carlson, Rev. Sci. Instrum. **50**, 1093 (1979).